Atomic-level insights into single-layer Co-promoted MoS2 clusters supported on a rutile TiO2(110) model oxide support

Prabhu, M.K.; Groot, I.M.N.

Citation
Prabhu, M. K., & Groot, I. M. N. (2024). Atomic-level insights into single-layer Co-promoted MoS2 clusters supported on a rutile TiO2(110) model oxide support. *Surface Science*, *739*. doi:10.1016/j.susc.2023.122385

Version: Publisher's Version
License: Creative Commons CC BY 4.0 license
Downloaded from: https://hdl.handle.net/1887/3730962

Note: To cite this publication please use the final published version (if applicable).

Surface Science 739 (2024) 122385

Contents lists available at ScienceDirect

Surface Science

journal homepage: www.elsevier.com/locate/susc

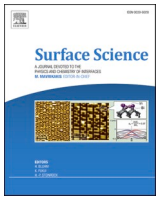

Atomic-level insights into single-layer Co-promoted MoS_2 clusters supported on a rutile TiO_2(110) model oxide support

M.K. Prabhu , I.M.N. Groot *

Gorlaeus Laboratories, Leiden Institute of Chemistry, Leiden University, Einsteinweg 55, 2333 CC Leiden, the Netherlands

ARTICLE INFO

Keywords:
Co-promoted MoS_2
STM
XPS
TiO_2(110)
TMDC

ABSTRACT

Single-layer mixed metal transition metal dichalcodenides (TMDCs), such as Co-promoted MoS_2 supported on metal oxide supports like TiO_2, have a wide range of applications in heterogeneous, electro- and photocatalysis, energy harvesting, and energy storage. In this work, we present atomic-level insights into the interaction between single-layer Co-promoted MoS_2 clusters and a model oxide rutile TiO_2(110) support. We have used physical vapor deposition (PVD) to synthesize a precursor containing bimetallic Co-Mo nanoparticles supported on (1 × 1) TiO_2(110). We sulfide this precursor using an H_2S background of 1×10^{-3} mbar at 650 K to synthesize the Co-promoted MoS_2 clusters. We use a combination of scanning tunneling microscopy (STM) and X-ray photoelectron spectroscopy (XPS) to analyze the Co-promoted MoS_2 clusters. We compare our results with that of pristine MoS_2 clusters supported on TiO_2(110), synthesized by an identical procedure, but without the Co atoms. We demonstrate that Co addition enhances the yield of (Co-promoted) MoS_2 clusters, in comparison to sulfidation of Mo nanoparticles to form MoS_2 clusters. Additionally, we also find that the Co-promoted MoS_2 clusters have predominantly high-index edge terminations which likely are stabilized by Co-S-Ti and Mo-S-Ti linkages to an (3 × 1) S-TiO_2 structure formed during the sulfidation. This causes an increase in the local density of states (LDOS) at the BRIM sites, thereby increasing their contrast in the STM images at the linkage sites. We have used our experimental results to propose a candidate atomic model for the Co-promoted MoS_2 clusters supported on TiO_2(110).

1. Introduction

To understand the atomic structure of surfaces, one of the very successful approaches has been to use a scanning tunneling microscope (STM) [1]. This technique provides the possibility to directly image the atomic structure of the active phase, especially when it is atomically-thin, such as for instance, a 2D material. This is very useful for catalysis research as it helps with relating the atomic structure of the catalyst to possible reaction mechanisms, structural and chemical changes of the active sites, and, ultimately, to the catalyst's activity and selectivity. STM especially, has been very useful for imaging the surface of 2D-material-based catalysts for hydrodesulfurization (HDS), a process that is very important for reducing global SO_x emissions and meeting the stringent emission standards [2,3].

A typical HDS catalyst used in the industry is based on sulfided Mo, Ni-Mo and Co-Mo nanoparticles supported on oxide supports like Al_2O_3 and TiO_2 [4–9]. The sulfidation process generates single-layer slabs of MoS_2 decorated with Ni or Co dopant atoms on the step edges [10,11]. So far, model HDS catalysts based on sulfided Mo, Ni-Mo and Co-Mo nanoparticles supported on Au(111) have been imaged using STM to gain insights into the atomic structure, location of dopant atoms, kinetics and chemistry of the active MoS_2 phase, and the effects of Ni and Co dopants [11–18]. Au(111) has been the choice substrate for this purpose as it is a chemically inert support with an atomic structure that has been well-studied, and also interacts relatively weakly with the pristine and promoted MoS_2 clusters, therefore allowing for the thermodynamic stability of the step edges to dominate their morphology. In order to understand the effect of the slab-support interactions, model oxide supports like rutile TiO_2(110) have been used as a convenient model support instead of Au(111) [19–24]. STM and atomic force microscopy (AFM) have been used to image pristine MoS_2 clusters supported on TiO_2(110) grown using low- and high-temperature synthesis strategies based on the sulfidation of Mo nanoparticles supported on TiO_2(110), and using a sulfiding agent like H_2S or elemental sulfur [19–24]. These studies have consistently shown that the MoS_2 slab morphologies are strongly influenced by the support interactions.

* Corresponding author.
E-mail address: i.m.n.groot@lic.leidenuniv.nl (I.M.N. Groot).

https://doi.org/10.1016/j.susc.2023.122385
Received 4 July 2023; Received in revised form 23 August 2023; Accepted 14 September 2023
Available online 17 September 2023
0039-6028/© 2023 The Author(s). Published by Elsevier B.V. This is an open access article under the CC BY license (http://creativecommons.org/licenses/by/4.0/).

However, atomic-level investigations using an STM on the role of promoter atoms on the shape and size of the single-layer MoS_2 clusters on a metal oxide support have not been explored so far. Furthermore, the exact nature of the single-layer metal sulfide-metal oxide support interactions that are catalytically relevant is poorly understood. This becomes a very important next step as many recent studies have shown that HDS catalysts based on strongly interacting supports like TiO_2 have a high activity for sulfur removal from sterically hindered aromatic molecules like thiophene derivatives which are the primary left-over sulfur contaminants in present-day commercial fuels [25–28].

In addition to heterogeneous catalysis, Co-doped MoS_2/TiO_2 junctions have been shown to have good catalytic activity for the hydrogen evolution reaction (HER), the oxygen evolution reaction (OER), and the oxygen reduction reaction (ORR) [29]. Transition-metal-doped MoS_2/TiO_2 nanocomposites also have potential applications for ammonia production by light-activated direct nitrogen fixation [30]. Transition metal doping of MoS_2/TiO_2 nanocomposites have been found to lower contact resistance to enhance transistor performance and photo-degeneration activity for breakdown of volatile organic compounds [31,32]. The doped and pristine MoS_2/TiO_2 junction architecture has also been explored for applications in broad-spectrum photocatalysis, lithium ion batteries, high-energy storage, hetero-structure supercapacitors, gas and liquid sensors, and selective CO_2 reduction electrodes [33–37]. Many of these enhanced chemical, optical, and physical properties of the MoS_2/TiO_2 system are linked to the atomic structure of the two layers and the interface between them, which in turn, is affected strongly by the precise growth conditions [38].

In this article, we have used STM to image single-layer Co-promoted MoS_2 clusters supported on rutile $TiO_2(110)$ to gain insights into the atomic structure and substrate interactions. We have also used X-ray photoelectron spectroscopy (XPS) to gain chemical insights into the effects of incorporating Co into the lattice of MoS_2 clusters. A synthesis strategy in which, Co and Mo nanoparticles are sequentially deposited on $TiO_2(110)$ using physical vapor deposition (PVD) to prepare a precursor containing purely Co-Mo bimetallic nanoparticles on $TiO_2(110)$ has been used. This precursor is then sulfided using H_2S to synthesize single-layer Co-promoted MoS_2 clusters. We compare the results to a control system containing pristine MoS_2 clusters on $TiO_2(110)$ grown at identical conditions. We find that the presence of Co increases the yield of Co-promoted MoS_2 clusters by enhancing the diffusion of sulfur without significantly influencing the overall size distribution. Furthermore, the Co-promoted MoS_2 clusters have irregular shapes with predominantly high-index edge terminations. The slabs adopting this shape are found to be commensurate with a (3×1) S-TiO_2 structure, which is expected to form at the H_2S background pressures used in this experiment [22], suggesting that the metal sulfide-support interactions dominate over the thermodynamic stability of the edges themselves, in determining the morphology of Co-promoted MoS_2 supported on rutile $TiO_2(110)$. We have presented a candidate atomic model to fit our experimental findings. Ultimately, our results provide fundamental insights into the atomic structure and interactions between Co-promoted MoS_2 clusters and the $TiO_2(110)$ substrate relevant for establishing atomic structure-activity relationships for catalysis, photochemistry, and electrochemistry associated with the Co-MoS_2/TiO_2 system.

2. Experimental methods

A rutile $TiO_2(110)$ single crystal was purchased from Surface Preparation Laboratory (SPL), Zaandam, the Netherlands. The surface of the $TiO_2(110)$ single crystal was cleaned with repeated cycles of sputtering with Ar^+(1.2 keV) and annealing (~900 K) in the analysis chamber of the ReactorSTM set up [39] based on a recipe detailed in our previous work [22] until the contaminations from the polishing were below the detection limits of the XPS and STM. This resulted in an atomically flat (1×1) $TiO_2(110)$ surface with a slightly blue color due to the formation of bulk O-vacancies rendering the single crystal conducting enough to perform STM measurements [40]. The background pressure of the system for all the experiments mentioned in this work was of the order of 10^{-10} mbar. The sample was mounted using tungsten clamps. Tungsten was used as it has a distinct XPS signal which is conveniently far from any Mo, S, or Ti signatures. Furthermore, the vapor pressure of W is far too low for any significant evaporation and cross contamination of the single crystal. Additionally, we also expect that any volatile W oxides, if formed, are etched away by the ion bombardment during the cleaning procedure and hence, do not contaminate the sample surface. The TiO_2 samples are always found to be free of W contamination within the detection limits of the XPS.

Mo and Co evaporation were carried out from an Oxford EGCO4 e-beam evaporator. The Mo and Co rods were purchased from Goodfellow and outgassed thoroughly before usage. The coverages of Mo and Co (reported as monolayers (ML) with respect to TiO_2) were measured by comparing the intensities of Mo 3d and Co $2p_{3/2}$ XPS spectra to that of the Ti 2p spectrum after taking into account the relative sensitivity factors, inelastic mean free path of electrons and emission depth distribution functions of TiO_2 [41–43]. For all the metal evaporation procedures, a counter voltage was applied on the pockets to deflect any metal ions produced. For preparing Mo nanoparticles alone on $TiO_2(110)$, Mo was evaporated with a flux of 0.02 ML/min onto a clean rutile $TiO_2(110)$ substrate held at room temperature to up to 0.2 ML coverage. For preparing bimetallic Co-Mo nanoparticles, Co was evaporated with a flux of 0.05 ML/min to up to 0.2 ML onto a sample containing 0.2 ML of Mo nanoparticles supported on the rutile $TiO_2(110)$ substrate held at room temperature. For preparing Co nanoparticles alone on $TiO_2(110)$, Co was evaporated with a flux of 0.05 ML/min onto a clean rutile $TiO_2(110)$ substrate held at room temperature to up to 0.14 ML coverage.

The sample containing bimetallic Co-Mo nanoparticles supported on $TiO_2(110)$ was used as the precursor for sulfidation based on a low-temperature recipe adapted from our previous work [22]. For synthesizing Co-promoted MoS_2 clusters, the sulfidation was carried out using H_2S gas as the sulfiding agent. The Co-Mo nanoparticles/$TiO_2(110)$ precursor was heated in 1×10^{-3} mbar of H_2S to 650 K and held at that temperature for 45 min. Thereafter, the sample was cooled to room temperature in UHV. For preparing pristine MoS_2 clusters as a control experiment, the Mo nanoparticles/$TiO_2(110)$ precursor was heated in 1×10^{-3} mbar of H_2S to 650 K and held at that temperature for 45 min. Thereafter, the sample was cooled to room temperature in UHV.

To regenerate the clean $TiO_2(110)$ surface after Mo and Co evaporation and subsequent sulfidation, the sample was cleaned by cycles of sputtering followed by annealing in oxygen (873 K, 1×10^{-5} mbar) to retain the residual Mo and Co on the surface following the Ar^+ ion bombardment. About 30 monolayers were removed before Mo, Co, and S were below the detection limit in the XPS. Annealing in UHV to 900 K to up to 10 min was performed in the last cleaning cycle to recover the clean (1×1) surface of $TiO_2(110)$.

Scanning tunneling microscopy (STM) in the ReactorSTM set up[39] was performed using STM tips made by cutting Pt-Ir 90–10 wires purchased from Goodfellow. The scans were performed in the UHV mode of the ReactorSTM at room temperature. All the STM images reported in this work were obtained using the constant-current mode using LPM video-rate scanning electronics described in detail elsewhere [44–46]. In-house developed Camera software was used for data acquisition and WSxM was used for STM image processing [47]. For obtaining the height profiles, a correctly connected surface was obtained using the most-common normal filtering method. Line-by-line background subtraction was carried out for obtaining sufficient contrast for viewing the surface features easily.

The XPS measurements were carried out using a SPECS Phoibos laboratory system equipped with an XRM50 X-ray source set to the Al K-alpha line (1486.8 eV) used along with a monochromator for excitation at an incidence angle of 55°. The XPS acquisition was carried out within the ReactorSTM set up itself without exposing the samples to air. The

XPS source was operated at 250 W with an acceleration voltage of 10 kV. The photoemission was analyzed using a HSA3500 hemispherical analyzer with a pass energy of 30 eV. The obtained spectra were integrated 20 times to obtain sufficiently high signal-to-noise ratio. The XPS spectra were calibrated by setting the bulk Ti 2p peak to 459.1 eV [48–50]. The calibration was further confirmed by checking that the Au 4f signal of a clean Au(111) single crystal was obtained at 84 eV. The XPSPEAK41 software was used for peak fitting the Mo 3d, Co $2p_{3/2}$, and Ti 2p spectra. All the fitting was done using mixed Gaussian-Lorentzian (65–35) curves. Shirley background subtraction was applied, and a non-linear least squares method was used for converging on to the solutions by constraining the peak positions to within ± 0.1 eV of the mean literature-reported value and solving for the peak area and peak width. In the case of satellites, the relative intensity ratio with respect to the main peak obtained from the literature was used as an additional constraint along with the peak position. The convergence of the solution was checked by using different initial conditions for the main peaks. The peak positions used for fitting are tabulated in Table 1.

3. Results and discussion

To prepare the Co-promoted MoS_2 clusters supported on rutile TiO_2(110), we first prepare a Co-Mo/TiO_2(110) precursor. First, Mo nanoparticles are grown on a clean rutile (1 × 1) TiO_2(110) substrate. Thereafter, Co nanoparticles are deposited onto the Mo/TiO_2(110) substrate at room temperature, as detailed in the experimental methods. Furthermore, a control sample containing only Co nanoparticles supported on an identically processed clean TiO_2(110) (without Mo) is prepared to gain insights into the chemistry of the Co-Mo/TiO_2 interactions.

Fig. 1a and b show the STM image and the Mo 3d XPS spectrum of Mo nanoparticles supported on TiO_2(110). Fig. 1a shows the presence of randomly nucleated Mo nanoclusters on the terraces of TiO_2(110). Most of the nanoparticles have a measured height in the range of 2–3.5 Å, while a few nanoparticles in the range of 5–6 Å are also observed (for height line A, see SI, Fig. S1). The exact diameters of the nanoparticles are difficult to determine, due to tip effects from the cut Pt-Ir wires. There is no preference for any nucleation sites along the steps or the terraces given the fully random nature of the Mo nucleation. Furthermore, the Mo nanoparticles consist of Mo in 4+ and less than 4+ oxidation state (denoted as MoO_x with $1 < x < 2$), suggesting a spontaneous oxidation of Mo (see Fig. 1b). We also observe the near-surface reduction of the TiO_2(110) substrate upon the deposition of Mo (See SI, Fig. S2). The spontaneous oxidation of Mo to Mo^{4+} and reduction of Ti^{4+} to Ti^{3+} is expected due to the thermodynamic favorability of this redox process and has been reported in the literature [51–54,68,69]. However, the complete oxidation of Mo to Mo^{4+} is kinetically limited at room temperature [51–54,68,69]. The results presented in Fig. 1a and 1b agree very well with prior reports of Mo nanoparticles synthesized on a TiO_2 substrate [51–54,68,69].

Fig. 1c shows the STM image of Co nanoparticles deposited on top of the sample containing Mo nanoparticles supported on TiO_2(110) (as in Fig. 1a) according to the recipe detailed in the experimental methods. Comparing Fig. 1c and a, we observe that the random distribution of nanoparticles in Fig. 1a is preserved in Fig. 1c. The nanoparticles are measured to be 4–5.6 Å high (For height line B in Fig. 1c, see SI, Fig. S1), suggesting an average increase in height of up to 2 Å upon Co deposition. Additionally, the Mo 3d XPS spectrum after the deposition of Co (Fig. 1d) shows a decrease in the Mo^{4+}component and an increase in the component for Mo in the less than 4+ oxidation state. This suggests that the interaction between Co and Mo leads to a slight reduction of the Mo nanoparticles. It is therefore, evident that the Mo nanoparticles generally act as pinning sites for the Co atoms. The Co $2p_{3/2}$ XPS spectrum in Fig. 1e shows that most of the Co is in the metallic state along with some Co^{2+} oxide. Furthermore, the Ti 2p XPS spectrum (SI, Fig. S2) for this sample shows an additional 2% increase in the amount of near-surface Ti^{3+}, suggesting a slight further reduction of TiO_2 upon the deposition of Co. The increase in the amount of Ti^{3+} upon the spontaneous oxidation of the Mo and Co strongly suggests a redox reaction involving charge transfer between the nanoparticles and the TiO_2 substrate.

As a comparison, when Co nanoparticles are grown on a freshly prepared TiO_2(110) substrate, we observe the formation of fewer but larger nanoparticles without a preference for a nucleation site (see Fig. 1f). The Co nanoparticles thus grown, have a height of 8–9 Å (see SI, Fig. S1). The formation of fewer but larger nanoparticles is attributed to the weaker interaction of Co with TiO_2 in comparison to Mo, and hence, a longer diffusion length [63,64,70–73]. This is because, the spontaneous partial oxidation of Mo to Mo^{4+} at the cost of the reduction of Ti^{4+} to Ti^{3+} is thermodynamically favorable, whereas, the formation of Co oxides is less favorable than the formation of TiO_2 [51,52,54,74]. Only the oxidation of the interfacial Co and a slight reduction of Ti^{4+} as a consequence have been reported in the literature [63]. In comparison to Fig. 1e, the Co $2p_{3/2}$ spectrum in Fig. 1g shows more metallic Co and less Co^{2+} oxide agreeing well with literature. The presence of more Co^{2+} oxide signature in Fig. 1e compared to Fig. 1g indicates that there more Co atoms at the interface, which agrees well with our STM observation that Co spreads more when Mo nanoparticles are present on the surface. The XPS spectra of Co $2p_{3/2}$ further demonstrate that the spontaneous oxidation of Co is limited to the interface only even when Mo nanoclusters are already present.

Typically, when bimetallic nanoparticles are synthesized on reducible oxide supports like TiO_2(110), the more reactive metal is deposited first. This allows the first metal to act as the nucleation site for the second less reactive metal, leading to a greater spreading of the second. Typically, the two metals are selected such that the first metal is highly reactive (such as Mo, Ni, Fe, Co) while the second is a noble metal (such as Pt, Pd, Au, Rh) [71,75–81]. This ensures that all the nanoparticles are

Table 1
Table of XPS peak positions used for peak fitting.

Component	Peak type	Peak position (eV)	ΔBE (eV)*	Reference
Mo metal	Mo $3d_{5/2}$	228	3.15	[51–59]
MoO_x	Mo $3d_{5/2}$	228.7	3.15	[51–59]
MoO_2	Mo $3d_{5/2}$	229.8	3.15	[51–59]
MoS_2	Mo $3d_{5/2}$	229.2	3.15	[51–59]
MoS_x (4 coordinated Mo)	Mo $3d_{5/2}$	228.3	3.15	[51–59]
MoS_x (5 coordinated Mo)	Mo $3d_{5/2}$	228.8	3.15	[51–59]
S	S 2s	226.2		[58–61]
Co metal	Co $2p_{3/2}$	778.1		[62–64]
Co metal satellite 1	Co $2p_{3/2}$	781.1		[62–64]
Co metal satellite 2	Co $2p_{3/2}$	783.1		[62–64]
Co^{2+} oxide	Co $2p_{3/2}$	779.9		[62–64]
Co^{2+} oxide satellite 1	Co $2p_{3/2}$	782		[62–64]
Co^{2+} oxide satellite 2	Co $2p_{3/2}$	785.4		[62–64]
Co^{2+} oxide satellite 3	Co $2p_{3/2}$	786.4		[62–64]
Co sulfide (Co_9S_8)	Co $2p_{3/2}$	777.8		[58,59,65–67]
Co sulfide satellite 1	Co $2p_{3/2}$	780.8		[58,59,65–67]
Co sulfide satellite 2	Co $2p_{3/2}$	782.8		[58,59,65–67]
Co Co-MoS_2	Co $2p_{3/2}$	778.5		[58,59,65–67]
Co Co-MoS_2 satellite 1	Co $2p_{3/2}$	781.5		[58,59,65–67]
Co Co-MoS_2 satellite 2	Co $2p_{3/2}$	783.5		[58,59,65–67]
TiO_2 (Ti^{4+})	Ti $2p_{3/2}$	459.1	5.7	[48,50]
TiO_x (Ti^{3+})	Ti $2p_{3/2}$	456.5	5.7	[48,50]

* ΔBE(3d) = BE $3d_{5/2}$ – BE $3d_{3/2}$, ΔBE(2p) = BE $2p_{3/2}$ – BE $2p_{1/2}$.

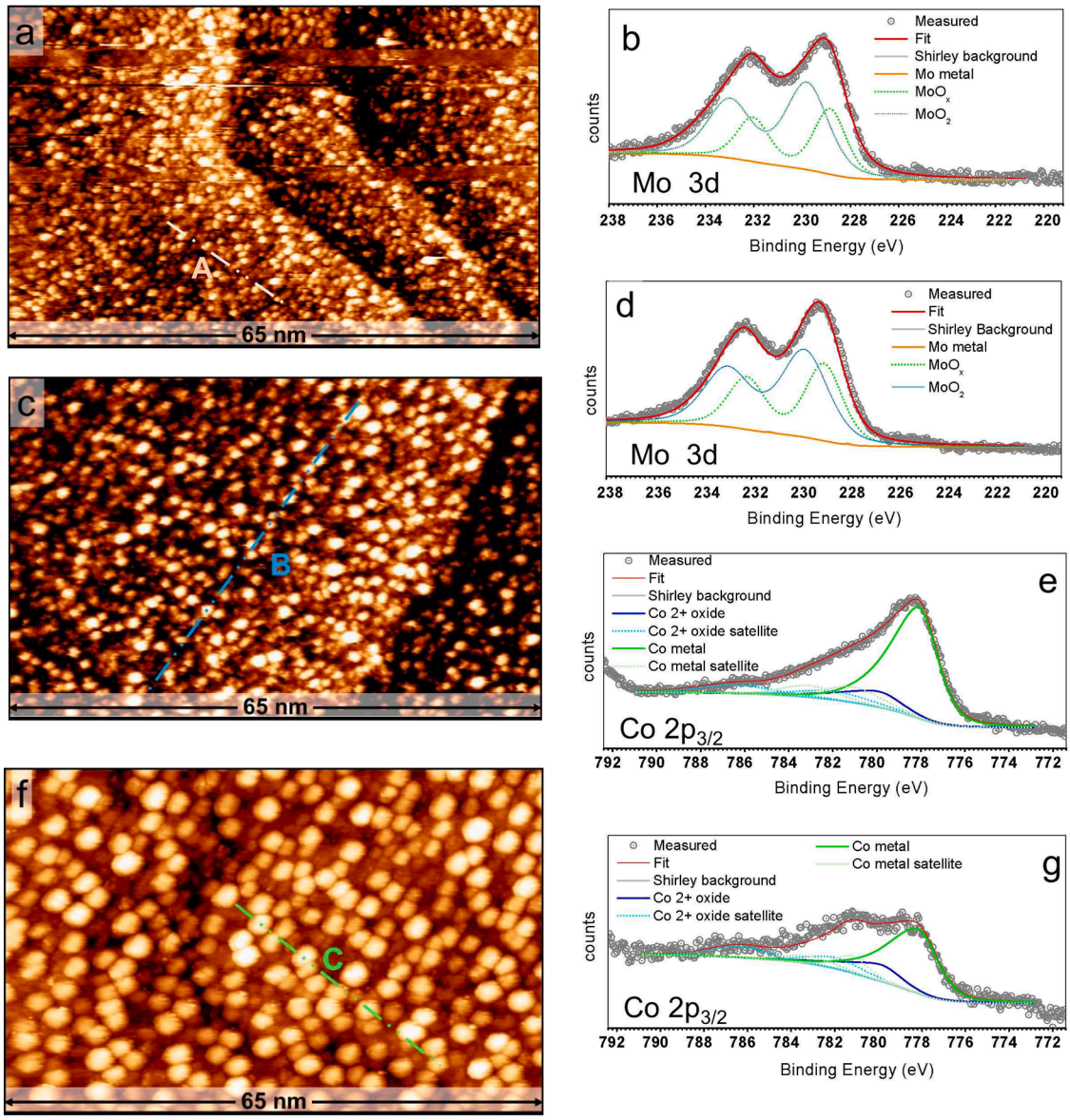

Fig. 1. a, c, f) STM images of Mo, Co-Mo, and Co nanoparticles on TiO_2(110), respectively, b, d) Mo 3d XPS spectrum of Mo and Co-Mo nanoparticles on TiO_2(110), respectively, e, g) Co $2p_{3/2}$ XPS spectrum of Co and Co-Mo nanoparticles on TiO_2(110), respectively. Measured height along the lines marked A, B and C in Fig. 1a, c and f are shown in SI, Fig. S1. STM images are acquired at +2.2 V, 100 pA.

bimetallic without phase separation. In our case, both Co and Mo are considered reactive with respect to noble metals, with Mo being reactive enough to partially oxidize spontaneously while Co undergoes spontaneous oxidation of the first atomic layer at the interface only. While our results show that the Mo nanoparticles act as nucleation sites for Co, we discuss several possibilities:

a) All the Mo nanoparticles contain Co. There is no new nucleation of Co nanoparticles.
b) All the Mo nanoparticles contain Co. There is some nucleation of additional Co nanoparticles also.
c) Some Mo nanoparticles do not contain Co. There is no new nucleation of Co nanoparticles.
d) Some Mo nanoparticles do not contain Co. There is some nucleation of Co nanoparticles also.

Given the uniform flux of Co atoms from the e-beam evaporator, we expect that all Mo nanoparticles are exposed to Co equally. Therefore, possibilities c) and d) are eliminated. In order to check whether there is new nucleation after Co deposition, statistical analysis of a large number of STM images is carried out to determine the number of nanoparticles per unit substrate area (see Table 2). We observe that the number density of the nanoparticles per 100 nm^2 substrate area is 37.82 ± 2.17 before Co deposition and 36.70 ± 1.47 after Co deposition, suggesting that new nanoparticles are not formed within the limits of the particle detection error. Therefore, the only possibility which satisfies the experimental observations is that of a), that is, all Mo nanoparticles must contain some Co. Additionally, comparison of the signal intensity of the Mo 3d spectra in Fig. 1b and d shows a 14.5% decrease in the intensity of Mo after Co deposition. This attenuation can only be explained if the Mo

Table 2
Statistical analysis of the number of particles after PVD of Co and Mo.

	Mo/TiO_2(110)	Co-Mo/TiO_2(110)
Total number of nanoparticles	36,094	46,407
Area analyzed (nm^2)	330,300	482,350
No. of particles / 100 nm^2 substrate area	37.82 ± 2.17	36.70 ± 1.47

nanoparticles are, in general, encapsulated by Co to some extent.

We, however, note the striking differences in the behavior of Co in the presence and absence of Mo nanoparticles. Based on thermodynamics arguments alone, we do not expect the reduction of Mo and Ti to occur upon the deposition of Co due to the lower heat of formation of Co oxide in comparison to Mo^{4+} oxide and Ti^{4+} oxide [51,52,54,74]. However, our experiment shows that oxidation of Co is more favorable only when there is greater spreading of Co. Therefore, we infer that the spontaneous oxidation of Co at the Co nanoparticle/Mo nanoparticle interface alone is favorable enough to slightly reduce both Mo and Ti

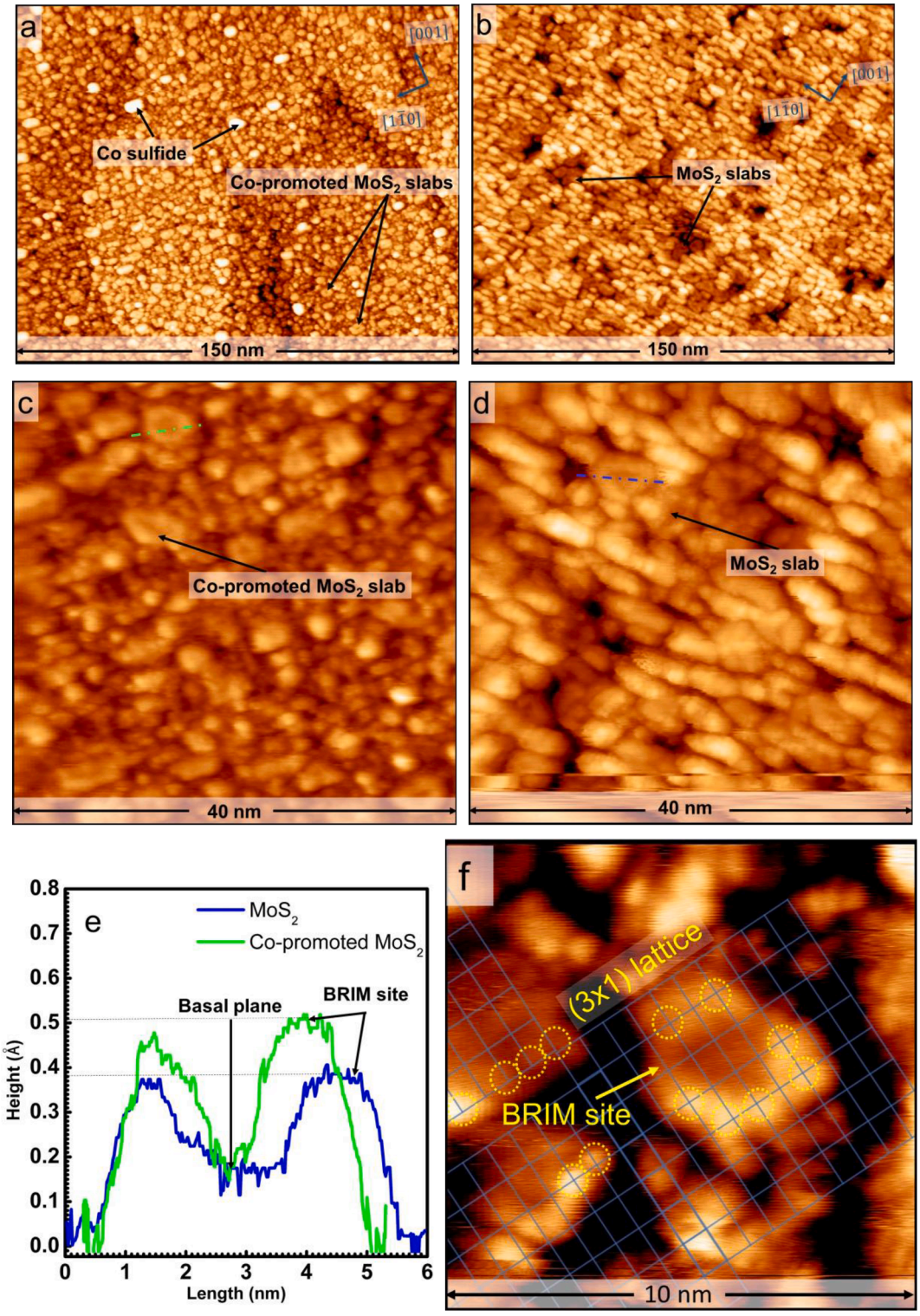

Fig. 2. a, c) STM images of Co-Mo nanoparticles on TiO_2(110) after sulfidation at 650 K for 45 min under 1×10^{-3} mbar H_2S, b, d) STM images of Mo nanoparticles on TiO_2(110) after sulfidation at 650 K for 45 min under 1×10^{-3} mbar H_2S, e) Measured height along the dashed lines marked blue and green in Fig. 4c and d showing the enhanced BRIM contrast of the Co-promoted MoS_2 slab in comparison to an MoS_2 slab, f) STM image of a Co-promoted MoS_2 slab with a 3×1 S-TiO_2(110) lattice drawn to scale. The dotted circles show the location of the bright edge features on the BRIM that are commensurate with the 3×1 lattice. All STM images were acquired at +2.2 V and 150 pA.

near the surface while the bulk oxidation of Co is not. In fact, it has been observed in previous studies that the addition of reactive metals like Co and Ni increases the reducibility of Mo oxides even though the formation of bulk oxides of these metals is less favorable [82–86]. This behavior has been linked to the strong favorability of the spontaneous oxidation, especially in the case of more reactive Ni than Co, at the interface only.

We note that in the interpretation of the XPS data, binding energies of the components reported by studies on similar sub-monolayer coverage films of Mo and Co are used, whenever possible. It is well-known that the binding energies of nanoclusters, especially in the limit of a few atoms, are very size dependent. Typically, there is an increase in the binding energies with increase in size [87,88]. We expect that such size effects contribute to additional uncertainties in the XPS interpretation. Nevertheless, the interpretation of the measured data provides a lower bound for the amount of oxidation in the Co, Mo, and Co-Mo nanoparticles. Additionally, the density of Mo and Co-Mo nanoparticles mentioned in Table 2 is obtained using detection methods involving the significant contrast differences between Mo and Co-Mo and the TiO_2 substrate. Due to the spreading of Mo, very small nanoclusters are formed, and precise identification can be difficult. To better understand the contrast difference with the TiO_2 substrate for the nanoparticle detection procedure, STM images with lower Mo nanoparticle coverage were used as a reference (see SI, S0).

We select the Co-Mo/TiO_2(110) precursor, thus prepared, for synthesizing the Co-promoted MoS_2 clusters. We also reproduce the experiment from our previous work [22] and prepare a precursor containing 0.2 ML Mo nanoparticles alone on TiO_2(110) as a control for the sulfidation process, so that insights into the effects of introducing Co can be gained. Fig. 2a and 2b show the large-scale STM images obtained after the sulfidation of the Co-Mo precursor and the control Mo precursor, respectively. In both cases, irregularly shaped atomically-flat slabs with a bright periphery are observed to form. We identify these slabs as single-layer Co-promoted MoS_2 clusters in the case of sulfiding the Co-Mo nanoparticles as in Fig. 2a and single-layer MoS_2 clusters in the case of sulfiding Mo nanoparticles as in Fig. 2b. A typical height profile of a Co-promoted MoS_2 nanocluster (see Fig. 2e) shows a basal plane thickness of 2.2–2.6 Å, which matches well with the height of single-layer MoS_2 clusters supported on TiO_2 reported in previous experimental works where it has been shown that sub-monolayer coverage of Mo nanoparticles up to ~0.4 ML form single-layer clusters upon sulfidation, owing to the layer-by-layer growth mode of pristine MoS_2 on TiO_2(110) [19–21]. Fig. 2a also shows the presence of very bright nanoparticles which are identified as those of 3D Co sulfide. These nanoparticles are further resolved and shown in the SI. Additionally, several elongated linear structures oriented along the $[1\bar{1}0]$ direction of the TiO_2 substrate can be seen in Fig. 2b. These features are not formed upon the sulfidation of Co-Mo precursor (Fig. 2a). These elongated structures are identified as the "edge-on" MoS_x stripes and are formed due to the diffusion limitations of both Mo and S, given the strong interaction of both Mo and S with the TiO_2 substrate and a lower sulfidation temperature. For a discussion on the structure of these elongated MoS_x stripes, we refer to our previous work [22].

Qualitative comparison of Fig. 2a and b shows that the presence of Co suppresses the formation of the MoS_x stripes. The Co-promoted MoS_2 (Fig. 2a) and MoS_2 clusters (Fig. 2b) are formed in a crowded fashion on the TiO_2(110) terraces, indicating that the Mo diffusion length is not significantly affected by the presence of Co during the sulfidation process. The statistical analysis of the Co-promoted MoS_2 and MoS_2 clusters is tabulated in Table 3. The presence of Co increases the yield of Co-promoted MoS_2 clusters obtained from sulfidation of the Mo by 108%, in comparison to sulfidation of the same amount of Mo nanoparticles without Co. Based on this observation, we propose that the presence of Co enhances the transport of S atoms on the surface, thereby partially overcoming the diffusion limitations for the formation of single-layer Co-promoted MoS_2. Co nanoparticles are known to undergo cluster diffusion in the presence of H_2S by forming Co_yS_z clusters, even at room temperature on metallic substrates like Au(111) [89]. A similar cluster diffusion mechanism could play a role on the TiO_2(110) substrate as well, especially given the high background of H_2S used. The promotional effect of Co on the formation of MoS_2 clusters was observed to a coverage of up to 0.08 ML (with Mo being 0.2 ML). Traces of Co did not have significant effects on the formation of MoS_2 clusters (see SI, S4).

Table 3
Analysis of Co-promoted MoS_2 and MoS_2 *clusters* in Fig. 2a and b.

Property	Co-promoted MoS_2	MoS_2
Coverage (vs. TiO_2) (Monolayers)	0.435	0.201
Average size (equivalent hexagon radii) (nm)	3.8 ± 1.2 [2134 slabs]	3.7 ± 1.6 [967 slabs]
Co sulfide coverage	0.084	0

Fig. 2c and d show the zoomed-in STM images of Co-promoted MoS_2 and MoS_2 clusters, respectively. Both slabs are observed to have a bright periphery. The bright periphery is attributed to the presence of metallic edge states known, by trademark, as BRIM sites [90–92]. The BRIM sites are the result of electronic states build up near the edges due the presence of polar step edges on the Co-promoted MoS_2 and MoS_2 clusters [91,92]. The BRIM sites are visible as an increase in the measured height on the edges of the slabs, as the STM directly measures the local density of states near the surface (see Fig. 2e). Measured heights in Fig. 2e show that the Co-promoted MoS_2 clusters have a much higher BRIM site contrast with respect to the basal plane in comparison to the MoS_2 clusters. We attribute the increase in the BRIM contrast of Co-promoted MoS_2 clusters with respect to MoS_2 clusters on TiO_2(110) to the electronic effects of Co incorporation on the edges. It is expected that substitution of Mo by Co, even if partially, influences the residual polarization of the cluster edges and hence, the BRIM contrasts. For instance, on the Au(111) support, Co-promoted MoS_2 clusters have a higher BRIM contrast as compared to pristine MoS_2 clusters because Co incorporation into the edges of MoS_2 causes an increase in the metallicity of the edges, leading to an increase of the edge local density of states [10,15].

In Fig. 2a, c, and f, the TiO_2(110)-supported Co-promoted MoS_2 clusters also have irregular shapes, indicating that the slabs have high-index edge terminations. In our previous work [22], we have shown that sulfidation with 1×10^{-3} mbar of H_2S partially sulfides the TiO_2(110) substrate, leading to the formation of a (3×1) S-TiO_2 structure on to which the pristine MoS_2 clusters are commensurate with, through edge Mo-S-Ti linkages. An identical (3×1) S-TiO_2 structure was also observed in research work by other groups concerning the reaction of elemental S with TiO_2 [60,61]. We proposed that the MoS_2 clusters adopt an irregular shape due to the substrate interactions dominating the thermodynamic stability of the edges alone which would otherwise lead to a hexagonal cluster shape based on the 2D Wulff construction of an MoS_2 cluster. Furthermore, these Mo-S-Ti linkage sites were observed to cause local enhancement of the local density of states (LDOS) at the BRIM sites. The Co-promoted MoS_2 clusters in our experiments also have very bright features along the edges in addition to the BRIM, as is shown by the yellow circles in Fig. 2f. Using a relatively high H_2S background of 1×10^{-3} mbar, we also find that a (3×1) structure forms on the TiO_2(110) surface due to the S-O exchange. The LEED pattern of this structure is shown in the SI, S5. In Fig. 2f, a rectangular lattice scaled to the (3×1) S-TiO_2 structure is overlaid on the Co-promoted MoS_2 clusters. Clearly, the locations of bright features at the BRIM of the Co-promoted MoS_2 clusters match very well with the (3×1) S-TiO_2 lattice suggesting that the irregular cluster shapes are due to anchoring via the edges to the underlying sulfur atoms of the S-TiO_2 structure. Furthermore, we also note that not all these edge features have the same contrast enhancement. This may be due to the presence of two types of edge sites, namely, Mo-S-Ti and Co-S-Ti sites, which contribute to different amounts of enhancement to the local LDOS at the BRIM. This possibility may be further investigated through density functional

theory (DFT)-based modeling, which is outside the scope of this experimental work.

To gain chemical insights into the samples, XPS analysis is used to analyze the oxidation states of Co and Mo before and after the sulfidation. Particularly, the Co $2p_{3/2}$ and Mo 3d spectra are fit with Gaussian-Lorentzian curves to de-convolute the XPS signals into the components according to the procedure detailed in the experimental methods. As a first step, we sulfide a sample containing 0.14 ML Co nanoparticles alone on TiO_2(110) at identical sulfidation conditions, in order to measure the signature of the Co sulfide formed. Fig. 3a shows the Co $2p_{3/2}$ spectra of Co sulfide. The Co $2p_{3/2}$ signature of this sulfide matches very well with the XPS signature of metallic Co_9S_8 supported on TiO_2 [58,59,67]. The Co $2p_{3/2}$ spectrum of the sulfided Co/TiO_2(110) is fit with a main asymmetric peak and two satellite peaks. The peak positions are tabulated in Table 1 in the experimental methods.

It is known that incorporation of Co on to the edges of MoS_2 results in a component that resembles the Co_9S_8 signal, but is blue shifted by 0.5 to 0.8 eV depending on the support interactions [28,93]. After sulfidation of the Co-Mo precursor, the measured Co $2p_{3/2}$ signal in Fig. 3a (bottom spectrum) shows an overall blue shift of 0.7 eV. We de-convolute the Co $2p_{3/2}$ XPS signature obtained after the sulfidation of the Co-Mo precursor with a component for Co_9S_8 (main peak at 777.8 eV) and a component for Co on the MoS_2 edges (main peak at 778.5 eV). Within the uncertainties of the fitting procedure, we find that up to 65.8% of the

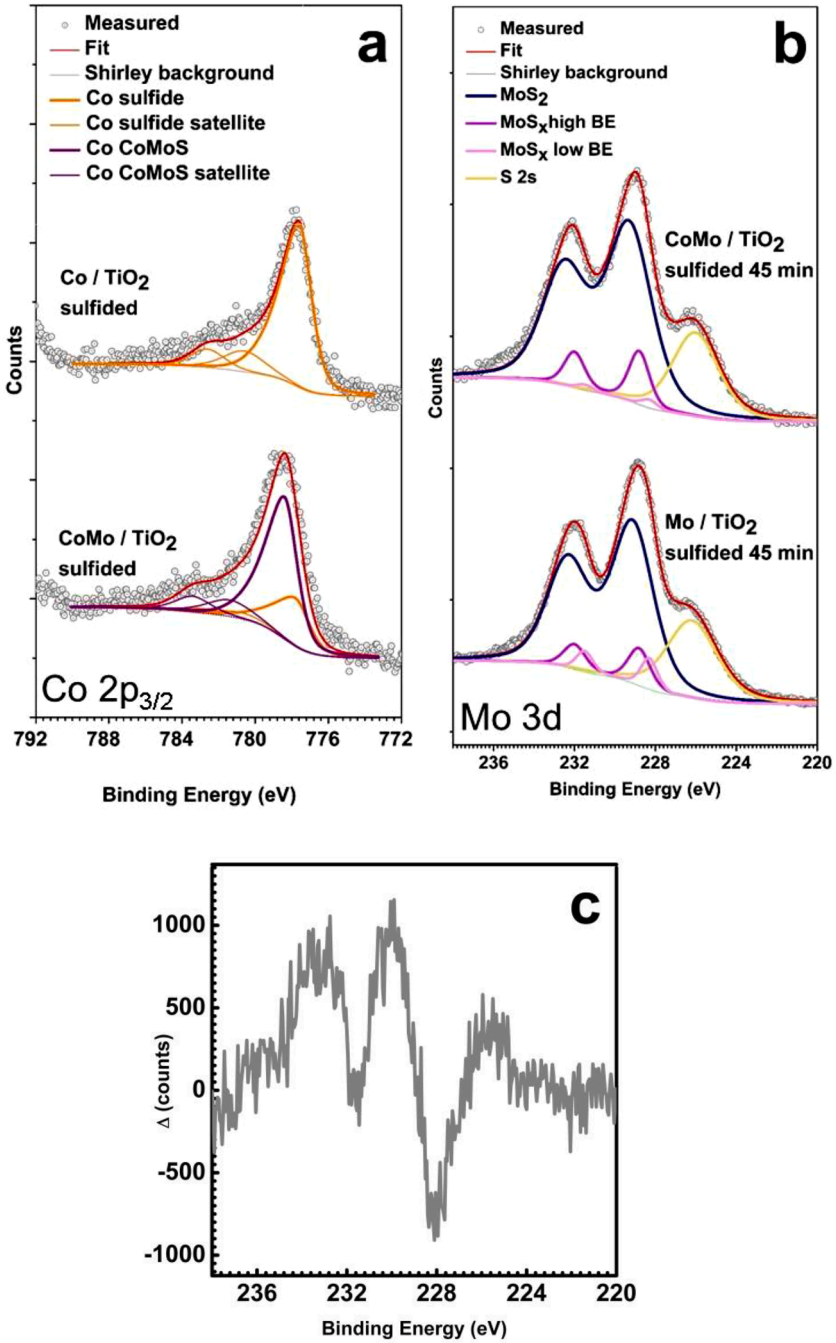

Fig. 3. a, b) Co $2p_{3/2}$ and Mo 3d spectra of Co-Mo and Mo nanoparticles supported on TiO_2(110) after sulfidation with H_2S. Co $2p_{3/2}$ spectrum of Co nanoparticles after sulfidation is also shown in a) for comparison, c) The difference between the Mo 3d spectra of Co-Mo nanoparticles and Mo nanoparticles after sulfidation with H_2S.

Co on the surface exists on the edges of MoS_2. This is in agreement with the STM image in Fig. 2a which shows that there is insufficient amount of Co_9S_8 nanoparticles to account for the 0.2 ML Co evaporated prior to sulfidation. Despite the larger diffusion length of Co in the presence of H_2S, the large number of Mo nanoparticles and MoS_2 clusters formed from them may act as pinning sites for the Co_yS_z diffusing clusters during the growth process, resulting in a higher yield of Co-promoted MoS_2.

The Mo 3d spectra of the Co-Mo and Mo nanoparticles after sulfidation are shown in Fig. 3b. The measured spectra are fit with components for Mo in the clustersof MoS_2, Mo in the elongated stripe phase, and Mo along the edges of the flat slabs along with the S 2s signature. We note that the Mo 3d spectra of both the Co-Mo precursor and Mo precursor are very similar. Therefore, to highlight the effects of Co addition, we also consider the difference between the Mo 3d signals of Co-Mo nanoparticles and Mo nanoparticles after sulfidation (see Fig. 3c). In Fig. 3c, it becomes clear that addition of Co causes an increase in the Mo signals around 229.9 and 233.2 eV which correspond to the $3d_{5/2}$ and $3d_{3/2}$ components of Mo^{4+} in the clusters of MoS_2 and Co-promoted MoS_2, while there is a decrease in the signal at 228.2 eV which corresponds to reduced Mo in the elongated stripe phase and coordinatively unsaturated Mo on the edges of the slabs. This can be explained by the increase in the yield of Co-promoted MoS_2 clusters and the absence of the elongated features upon addition of Co, as well as the decreased edge occupancy of Mo atoms due to Co substitution, all of which are in good agreement with the STM results. For the corresponding Ti 2p and S 2p spectra, we refer to the SI, Fig. S2.

Based on the well-agreeing STM and XPS results, we propose an atomic model for the Co-promoted MoS_2 clusters supported on $TiO_2(110)$. As an example, we consider the Co-promoted MoS_2 slab in Fig. 2f. For simplicity, we assume that all edge Mo atoms are substituted by Co. Given the observation from the STM images that the Co-promoted MoS_2 clusters are oriented along the $[1\bar{1}0]$ direction, we propose the atomic model shown in Fig. 4a. A 3D rendered STM image of this slab is shown in Fig. 4b. According to this atomic model, one pair of opposite sides of the Co-promoted MoS_2 slab are oriented along the $[1\bar{1}0]$ direction of the (3×1) S-TiO_2 structure while the remaining edges demonstrate higher-index terminations. The Mo atoms (violet) along the edges and corners are also substituted by Co, shown in blue. The terminating S edge atoms of the lower basal plane, shown in green, are proposed to interact through direct bonding to the (3×1) S-TiO_2 structure. The other S edge atoms may interact with the 4- and 5-fold coordinated Ti atoms on the surface. According to this model, twice the S-S distance in a Co-promoted MoS_2 slab matches closely with the distance between the Ti rows of the (3×1) S-TiO_2 structure (6.24 Å), thus allowing for maximum edge S-substrate Ti interactions. As a final comparison, Fig. 4a and 4b are overlaid in Fig. 4c to demonstrate a one-to-one match between the location of the Co-S-Ti sites and the bright BRIM features of the Co-promoted MoS_2 slab.

We note that an assumption of 100% edge substitution by Co is made in our atomic model for simplicity. Based on the STM images presented

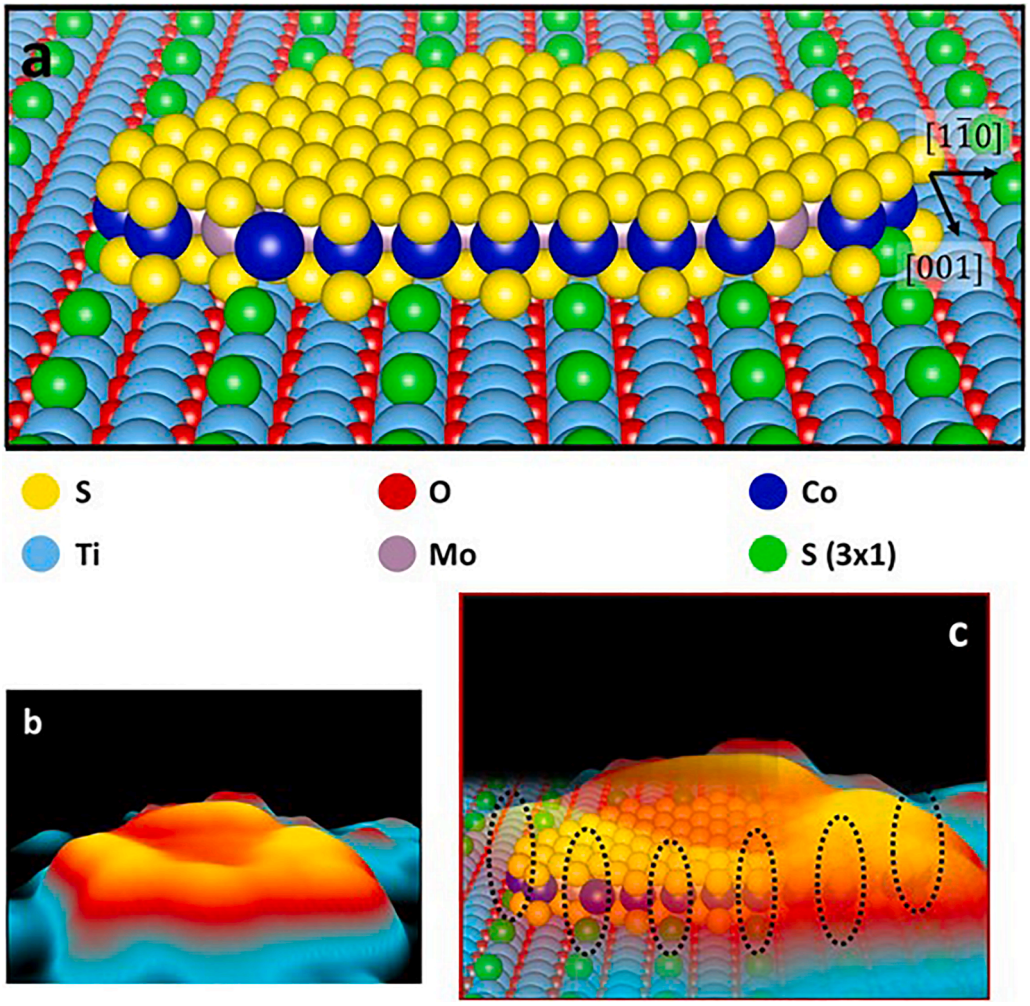

Fig. 4. a) Atomic model of the Co-promoted MoS_2 slab on $TiO_2(110)$, b) 3D rendered STM image of Co-promoted MoS_2 slab from Fig. 2f, c) Fig. 4b overlayed on top of Fig. 4a to show the match between corner sites and the brightest edge features in the STM image. The dotted circles highlight the location of the Co-S-Ti linkages in the model.

in this work, presence of both Mo and Co on the edges is very likely. Additionally, Co doping of the MoS_2 (without any ion bombardment) typically occurs via the edge substitution of Mo by Co, due to the thermodynamic stability of this location of Co [11]. To experimentally determine the precise location and configuration of the Co, atomic resolution, dI/dV spectroscopy, and supporting DFT calculations are necessary. Unfortunately, due to instrumental challenges, dI/dV spectroscopy is not possible on the ReactorSTM at the time of this work. Atomic resolution of the edges with the low-temperature synthesis is difficult to obtain due to the large number of diffusing sulfur species still remaining on the surface. To obtain better resolution, one may anneal the sample to ~900 K to desorb any excess sulfur, but this will cause irreversible morphological changes to the surface, such as sintering of the Co-MoS_2 clusters. DFT calculations involving large atomic models with a few thousand atoms taking into account irregular slabs of Co-MoS_2 including the TiO_2 surface with the (3×1)-S structure, such as the candidate atomic model presented in this work, are necessary in the future to better understand the state of Co on the edges of the Co-MoS_2 nanoclusters and the interaction with the S-TiO_2 support.

4. Conclusions

We have imaged and analyzed Co-promoted MoS_2 clusters supported on a model metal oxide rutile TiO_2(110) substrate using STM and XPS. The Co-promoted MoS_2 clusters were synthesized by sulfiding a Co-Mo bimetallic nanoparticle supported on TiO_2(110) using H_2S gas at a temperature of 650 K. The Co-promoted MoS_2 clusters are compared with pristine MoS_2 clusters synthesized by an identical procedure. Our STM and XPS results show that the presence of Co during the sulfidation process enhances the yield of Co-promoted MoS_2 clusters by increasing the diffusion of S atoms while limiting the formation of other Mo sulfide structures formed due to the diffusion limitations of Mo and S without Co. The Co-promoted MoS_2 clusters contain sites along the edges which appear bright in the STM images and are commensurate with a (3×1) S-TiO_2 structure. These sites are interpreted as locations of both Mo-S-Ti and Co-S-Ti linkages, as such strong interactions with the substrate can further explain the local enhancement of the LDOS at the edges and the irregular shapes of the Co-promoted MoS_2 clusters. We present a candidate atomic model based on our findings for possible future theoretical modeling. In summary, we provide atomic-level insights into the 2D material-metal oxide support interactions which are very useful for obtaining a fundamental understanding of the physical and chemical properties of this system that are useful for a wide range of applications in catalysis and energy storage and harvesting.

CRediT authorship contribution statement

M.K. Prabhu: Conceptualization, Formal analysis, Investigation, Methodology, Visualization, Writing – original draft, Writing – review & editing. **I.M.N. Groot:** Data curation, Funding acquisition, Methodology, Project administration, Resources, Software, Supervision, Validation, Writing – review & editing.

Declaration of Competing Interest

The authors declare that they have no known competing financial interests or personal relationships that could have appeared to influence the work reported in this paper.

Data availability

Data will be made available on request.

Supplementary materials

Supplementary material associated with this article can be found, in the online version, at doi:10.1016/j.susc.2023.122385.

References

[1] F. Tao, P.A. Crozier, Atomic-scale observations of catalyst structures under reaction conditions and during catalysis, Chem. Rev. (2016) 3487–3539.
[2] J.V. Lauritsen, F. Besenbacher, Atom-resolved scanning tunneling microscopy investigations of molecular adsorption on MoS_2 and CoMoS hydrodesulfurization catalysts dedicated to Haldor Topsøe, J. Catal. 328 (2015) 49–58.
[3] R.V. Mom, J.N. Louwen, J.W.M. Frenken, I.M.N. Groot, *In situ* observations of an active MoS_2 model hydrodesulfurization catalyst, Nat. Commun (1) (2019) 10.
[4] I. Shafiq, S. Shafique, P. Akhter, W. Yang, M. Hussain, Recent developments in alumina supported hydrodesulfurization catalysts for the production of sulfur-free refinery products: a technical review, Catal. Rev. Sci. Eng. 64 (1) (2022) 1–86.
[5] A. Tougerti, P. Simon, C. Desjacques, J.S. Girardon, F. Mazzanti, S. Pipolo, M. Trentesaux, S. Cristol, Rethinking electronic and geometric structures of real hydrodesulfurization catalysts by *in situ* photon-in/photon-out spectroscopy, J. Phys. Chem. C 124 (32) (2020) 17586–17598.
[6] C. Song, X. Ma, New design approaches to ultra-clean diesel fuels by deep desulfurization and deep dearomatization, Appl. Catal. B 41 (2003) 207–238.
[7] S. Brunet, D. Mey, G. Pérot, C. Bouchy, F. Diehl, On the hydrodesulfurization of FCC gasoline: a review, Appl. Catal. A (2005) 143–172.
[8] I.V. Babich, J.A. Moulijn, Science and technology of novel processes for deep desulfurization of oil refinery streams: a review, Fuel (2003) 607–631.
[9] B.M. Vogelaar, P. Steiner, T.F. van der Zijden, A.D. van Langeveld, S. Eijsbouts, J. A. Moulijn, Catalyst deactivation during thiophene HDS: the role of structural sulfur, Appl. Catal. A Gen. 318 (2007) 28–36.
[10] J.V. Lauritsen, J. Kibsgaard, G.H. Olesen, P.G. Moses, B. Hinnemann, S. Helveg, J. K. Nørskov, B.S. Clausen, H. Topsøe, E. Lægsgaard, F. Besenbacher, Location and coordination of promoter atoms in Co- and Ni-promoted MoS_2-based hydrotreating catalysts, J. Catal. 249 (2) (2007) 220–233.
[11] Y. Zhu, Q.M. Ramasse, M. Brorson, P.G. Moses, L.P. Hansen, H. Topsøe, C. F. Kisielowski, S. Helveg, Location of Co and Ni promoter atoms in multi-layer MoS_2 nanocrystals for hydrotreating catalysis, Catal. Today 261 (2016) 75–81.
[12] S. Helveg, J.V. Lauritsen, E. Lægsgaard, I. Stensgaard, J.K. Nørskov, B.S. Clausen, H. Topsøe, F. Besenbacher, Atomic-scale structure of single-layer MoS_2 nanoclusters, Phys. Rev. Lett. 84 (5) (2000) 951–954.
[13] J. Kibsgaard, J.V. Lauritsen, E. Lægsgaard, B.S. Clausen, H. Topsøe, F. Besenbacher, Cluster-support interactions and morphology of MoS_2 nanoclusters in a graphite-supported hydrotreating model catalyst, J. Am. Chem. Soc. 128 (42) (2006) 13950–13958.
[14] J.V. Lauritsen, M. Nyberg, R.T. Vang, M.V. Bollinger, B.S. Clausen, H. Topsøe, K. W. Jacobsen, E. Lægsgaard, J.K. Nørskov, F. Besenbacher, Chemistry of one-dimensional metallic edge states in MoS_2 nanoclusters, Nanotechnology 14 (3) (2003) 385–389.
[15] S.S. Grønborg, N. Salazar, A. Bruix, J. Rodríguez-Fernández, S.D. Thomsen, B. Hammer, J.V. Lauritsen, Visualizing hydrogen-induced reshaping and edge activation in MoS_2 and Co-promoted MoS_2 catalyst clusters, Nat. Commun. 9 (1) (2018) 1–11.
[16] N. Salazar, S.B. Schmidt, J.V. Lauritsen, Adsorption of nitrogenous inhibitor molecules on MoS_2 and CoMoS hydrodesulfurization catalysts particles investigated by scanning tunneling microscopy, J. Catal. 370 (2019) 232–240.
[17] A.K. Tuxen, H.G. Füchtbauer, B. Temel, B. Hinnemann, H. Topsoe, K.G. Knudsen, F. Besenbacher, J.V. Lauritsen, Atomic-scale insight into adsorption of sterically hindered dibenzothiophenes on MoS 2 and Co-Mo-S hydrotreating catalysts, J. Catal. 295 (2012) 146–154.
[18] A. Tuxen, J. Kibsgaard, H. Gøbel, E. Lægsgaard, H. Topsøe, J.V. Lauritsen, F. Besenbacher, Size threshold in the dibenzothiophene adsorption on MoS_2 nanoclusters, ACS Nano 4 (8) (2010) 4677–4682.
[19] R.P. Galhenage, H. Yan, T.B. Rawal, D. Le, A.J. Brandt, T.D. Maddumapatabandi, N. Nguyen, T.S. Rahman, D.A. Chen, MoS_2 nanoclusters grown on TiO_2: evidence for new adsorption sites at edges and sulfur vacancies, J. Phys. Chem. C 123 (12) (2019) 7185–7201.
[20] J. Kibsgaard, B.S. Clausen, H. Topsøe, E. Lægsgaard, J.V. Lauritsen, F. Besenbacher, Scanning tunneling microscopy studies of TiO_2-supported hydrotreating catalysts: anisotropic particle shapes by edge-specific MoS_2-support bonding, J. Catal. 263 (1) (2009) 98–103.
[21] H. Liu, Y. Li, M. Xiang, H. Zeng, X. Shao, Single-layered MoS_2 directly grown on rutile TiO_2(110) for enhanced interfacial charge transfer, ACS Nano 13 (5) (2019) 6083–6089.
[22] M.K. Prabhu, I.M.N. Groot, Low-temperature synthesis strategy for MoS_2 slabs supported on TiO_2(110), Surfaces 3 (4) (2020) 605–621.
[23] H. Uetsuka, H. Onishi, S. Ikeda, Y. Harada, H. Sakama, Y. Sakashita, Atomic force microscope observation of MoS_2 particles synthesized on mica, MoS_2, and graphite, e-J. Surf. Sci. Nanotechnol. 1 (2003) 80–83.
[24] H. Uetsuka, H. Onishi, Y. Harada, H. Sakama, Y. Sakashita, Microscope observation of MoS_2 nanoparticles synthesized on rutile TiO_2 single crystals, e-J. Surf. Sci. Nanotechnol 2 (2004) 32–37.
[25] E. Dominguez Garcia, J. Chen, E. Oliviero, L. Oliviero, F. Maugé, New insight into the support effect on HDS catalysts: evidence for the role of Mo-support interaction on the MoS_2 slab morphology, Appl. Catal. B Environ. 260 (2020), 117975.

[26] J.N.D. de León, C.R. Kumar, J. Antúnez-García, S. Fuentes-Moyado, Recent insights in transition metal sulfide hydrodesulfurization catalysts for the production of ultra low sulfur diesel: a short review, Catalysts (2019) 87.

[27] M. Breysse, C. Geantet, P. Afanasiev, J. Blanchard, M. Vrinat, Recent studies on the preparation, activation and design of active phases and supports of hydrotreating catalysts, Catal. Today 130 (1) (2008) 3–13.

[28] J. Ramírez, G. Macías, L. Cedeño, A. Gutiérrez-Alejandre, R. Cuevas, P. Castillo, The role of titania in supported Mo, CoMo, NiMo, and NiW hydrodesulfurization catalysts: analysis of past and new evidences, Catal. Today 98 (2004) 19–30.

[29] D.C. Nguyen, T.L. Luyen Doan, S. Prabhakaran, D.T. Tran, D.H. Kim, J.H. Lee, N. H Kim, Hierarchical Co and Nb Dual-Doped MoS_2 nanosheets shelled micro-TiO_2 Hollow Spheres as Effective multifunctional electrocatalysts for HER, OER, and ORR, Nano Energy (2021).

[30] Q. Song, C. Sun, Z. Wang, X. Bai, K. Wu, Q. Li, H. Zhang, L. Zhou, H. Pang, Y. Liang, S. Yue, Z. Zhao, Directed charge transfer in all solid state heterojunction of Fe Doped MoS_2 and C–TiO_2 nanosheet for enhanced nitrogen photofixation, Mater. Today Phys. (2021).

[31] N. Kaushik, D. Karmakar, A. Nipane, S. Karande, S. Lodha, Interfacial N-doping using an ultrathin TiO_2 layer for contact resistance reduction in MoS_2, ACS Appl. Mater. Interfaces (2016).

[32] X. Tang, Z. Wang, W. Huang, Q. Jing, N. Liu, Construction of N-doped TiO_2/MoS_2 heterojunction with synergistic effect for enhanced visible photodegradation activity, Mater. Res. Bull. (2018).

[33] H. Zhou, P. Lv, X. Xia, J. Zhang, J. Yu, Z. Pang, H. Qiao, Q. Wei, MoS_2 nanograins Doped TiO_2 nanofibers as intensified anodes for lithium ion batteries, Mater. Lett. (2018).

[34] X. Hu, S. Lu, J. Tian, N. Wei, X. Song, X. Wang, H. Cui, The selective deposition of MoS_2 nanosheets onto (101) facets of TiO_2 nanosheets with exposed (001) facets and their enhanced photocatalytic H2 production, Appl. Catal. B Environ. (2019).

[35] W. Ou, J. Pan, Y. Liu, S. Li, H. Li, W. Zhao, J. Wang, C. Song, Y. Zheng, C. Li, Two-dimensional ultrathin MoS_2-modified black Ti^{3+}–TiO_2 nanotubes for enhanced photocatalytic water splitting hydrogen production, J. Energy Chem. (2020).

[36] M. Iqbal, N.G. Saykar, A. Arya, I. Banerjee, P.S. Alegaonkar, S.K. Mahapatra, High-performance supercapacitor based on MoS_2@TiO_2 composite for wide range temperature application, J. Alloys Compd. (2021).

[37] A. Hezam, K. Alkanad, M.A. Bajiri, J. Strunk, K. Takahashi, Q.A. Drmosh, N. Al-Zaqri, L.N Krishnappagowda, 2D/1D MoS_2/tio_2 heterostructure photocatalyst with a switchable CO2 reduction product, Small Methods (2023).

[38] Y. Araki, K. Honna, H. Shimada, Formation and catalytic properties of edge-bonded molybdenum sulfide catalysts on TiO_2, J. Catal. (2002).

[39] C.T. Herbschleb, P.C. Van Der Tuijn, S.B. Roobol, V. Navarro, J.W. Bakker, Q. Liu, D. Stoltz, M.E. Cañas-Ventura, G. Verdoes, M.A. Van Spronsen, M. Bergman, L. Crama, I. Taminiau, A. Ofitserov, G.J.C. Van Baarle, J.W.M Frenken, The ReactorSTM: atomically resolved scanning tunneling microscopy under high-pressure, high-temperature catalytic reaction conditions, Rev. Sci. Instrum 85 (8) (2014) 83703.

[40] U. Diebold, M. Li, O. Dulub, E.L.D. Hebenstreit, W. Hebenstreit, The relationship between bulk and surface properties of rutile TiO_2(110), Surf. Rev. Lett. 7 (2000) 613–617.

[41] C.D. Wagner, Sensitivity factors for XPS analysis of surface atoms, J. Electron Spectros. Relat. Phenomena 32 (2) (1983) 99–102.

[42] G.C. Smith, A.B. Hopwood, K.J. Titchener, Electron inelastic mean free path for Ti, TiC, TiN and TiO_2 as determined by quantitative reflection electron energy-loss spectroscopy, Surf. Interface Anal. 33 (3) (2002) 230–237.

[43] H. Ota, M. Shimomura, F. Matsui, Separation of surface- and bulk-specific Ti L-edge XANES spectra of rutile (110) surface, J. Phys. Soc. Jpn. (1) (2018) 87.

[44] M.J. Rost, L. Crama, P. Schakel, E. Van Tol, G.B.E.M. Van Velzen-Williams, C. F. Overgauw, H. Ter Horst, H. Dekker, B. Okhuijsen, M. Seynen, A. Vijftigschild, P. Han, A.J. Katan, K. Schoots, R. Schumm, W. Van Loo, T.H. Oosterkamp, J.W. M Frenken, Scanning probe microscopes go video rate and beyond, Rev. Sci. Instrum. 76 (5) (2005), 053710.

[45] A. Hjorth Larsen, J. JØrgen Mortensen, J. Blomqvist, I.E. Castelli, R. Christensen, M. Dułak, J. Friis, M.N. Groves, B. Hammer, C. Hargus, E.D. Hermes, P.C. Jennings, P. Bjerre Jensen, J. Kermode, J.R. Kitchin, E. Leonhard Kolsbjerg, J. Kubal, K. Kaasbjerg, S. Lysgaard, J. Bergmann Maronsson, T. Maxson, T. Olsen, L. Pastewka, A. Peterson, C. Rostgaard, J. SchiØtz, O. Schütt, M. Strange, K. S. Thygesen, T. Vegge, L. Vilhelmsen, M. Walter, Z. Zeng, K.W. Jacobsen, The atomic simulation environment - a python library for working with atoms, J. Phys. Condens. Matter (2017).

[46] M.J. Rost, G.J.C. van Baarle, A.J. Katan, W.M. van Spengen, P. Schakel, W.A. van Loo, T.H. Oosterkamp, J.W.M. Frenken, Video-rate scanning probe control challenges: setting the stage for a microscopy revolution, Asian J. Control 11 (2) (2009) 110–129.

[47] I. Horcas, R. Fernández, J.M. Gómez-Rodríguez, J. Colchero, J. Gómez-Herrero, A. M. Baro, WSXM: a software for scanning probe microscopy and a tool for nanotechnology, Rev. Sci. Instrum. 78 (1) (2007), 013705.

[48] U. Diebold, T.E. Madey, TiO_2 by XPS, Surf. Sci. Spectra 4 (3) (1998) 227–231.

[49] M. Bowker, R. Sharpe, Pd deposition on TiO_2(110) and nanoparticle encapsulation, Catal. Struct. React. 1 (3) (2015) 140–145.

[50] J.T. Mayer, U. Diebold, T.E. Madey, E. Garfunkel, Titanium and reduced titania overlayers on titanium dioxide(110), J. Electron Spectros. Relat. Phenomena 73 (1) (1995) 1–11.

[51] B. Domenichini, S. Pétigny, V. Blondeau-Patissier, A. Steinbrunn, S. Bourgeois, Effect of the surface stoichiometry on the interaction of Mo with TiO_2 (110), Surf. Sci. 468 (1–3) (2000) 192–202.

[52] V. Blondeau-Patissier, G.D. Lian, B. Domenichini, A. Steinbrunn, S. Bourgeois, E. C. Dickey, Molybdenum thin-film growth on rutile titanium dioxide (1 1 0), Surf. Sci. 506 (1–2) (2002) 119–128.

[53] J. Prunier, B. Domenichini, Z. Li, P.J. Møller, S. Bourgeois, A photoemission study of molybdenum hexacarbonyl adsorption and decomposition on TiO_2(1 1 0) surface, Surf. Sci. 601 (4) (2007) 1144–1152.

[54] B. Domenichini, M. Petukhov, G.A. Rizzi, M. Sambi, S. Bourgeois, G. Granozzi, Epitaxial growth of molybdenum on TiO_2(1 1 0), Surf. Sci. 544 (2–3) (2003) 135–146.

[55] M. Dendzik, M. Michiardi, C. Sanders, M. Bianchi, J.A. Miwa, S.S. Grønborg, J. V. Lauritsen, A. Bruix, B. Hammer, P. Hofmann, Growth and electronic structure of epitaxial single-layer WS2 on Au(111), Phys. Rev. B - Condens. Matter Mater. Phys (24) (2015) 92.

[56] A. Bruix, H.G. Füchtbauer, A.K. Tuxen, A.S. Walton, M. Andersen, S. Porsgaard, F. Besenbacher, B. Hammer, J.V Lauritsen, *In situ* detection of active edge sites in single-layer MoS_2 catalysts, ACS Nano 9 (9) (2015) 9322–9330.

[57] T. Weber, J.C. Muijsers, J.H.M.C. Van Wolput, C.P.J. Verhagen, J. W. Niemantsverdriet, Basic reaction steps in the sulfidation of crystalline MoO3 to MoS_2, as studied by X-Ray photoelectron and infrared emission spectroscopy, J. Phys. Chem. 100 (33) (1996) 14144–14150.

[58] G.M. Bremmer, L. van Haandel, E.J.M. Hensen, J.W.M. Frenken, P.J. Kooyman, The effect of oxidation and resulfidation on (Ni/Co)MoS_2 hydrodesulfurisation catalysts, Appl. Catal. B Environ. 243 (2019) 145–150.

[59] G.M. Bremmer, L. Van Haandel, E.J.M. Hensen, J.W.M. Frenken, P.J. Kooyman, Instability of $NiMoS_2$ and $CoMoS_2$ hydrodesulfurization catalysts at ambient conditions: a quasi *in situ* high-resolution transmission electron microscopy and X-Ray photoelectron spectroscopy study, J. Phys. Chem. C 120 (34) (2016) 19204–19211.

[60] E.L.D. Hebenstreit, W. Hebenstreit, U. Diebold, Adsorption of Sulfur on TiO_2(110) Studied with STM, LEED and XPS: temperature-dependent change of adsorption site combined with O-S exchange, Surf. Sci. 461 (1–3) (2000) 87–97.

[61] E.L.D. Hebenstreit, W. Hebenstreit, U. Diebold, Structures of sulfur on TiO_2(1 1 0) determined by scanning tunneling microscopy, X-ray photoelectron spectroscopy and low-energy electron diffraction, Surf. Sci. 470 (3) (2001) 347–360.

[62] M.C. Biesinger, B.P. Payne, A.P. Grosvenor, L.W.M. Lau, A.R. Gerson, R.S.C Smart, Resolving surface chemical States in XPS analysis of first row transition metals, oxides and hydroxides: Cr, Mn, Fe, Co and Ni, Appl. Surf. Sci. 257 (7) (2011) 2717–2730.

[63] Muller, S. Synchrotron radiation spectroscopy studies of the initial interaction of chromium and cobalt with the surface of titanium dioxide, 1980.

[64] Y. Shao, W. Chen, E. Wold, J. Paul, Dispersion and electronic structure of TiO_2-supported cobalt and cobalt oxide, Langmuir 10 (1) (1994) 178–187.

[65] M.K. Prabhu, D. Boden, M.J. Rost, J. Meyer, I.M.N Groot, Structural characterization of a novel two-dimensional material: cobalt sulfide sheets on Au (111), J. Phys. Chem. Lett 11 (21) (2020) 9038–9044.

[66] M.K. Prabhu, I.M.N Groot, Simultaneous sulfidation of Mo and Co oxides supported on Au(111), Phys. Chem. Chem. Phys. 23 (14) (2021) 8403–8412.

[67] A.D. Gandubert, E. Krebs, C. Legens, D. Costa, D. Guillaume, P. Raybaud, Optimal promoter edge decoration of CoMoS catalysts: a combined theoretical and experimental study, Catal. Today 130 (1) (2008) 149–159.

[68] J.R. Kitchin, M.A. Barteau, J.G. Chen, A comparison of gold and molybdenum nanoparticles on TiO_2(1 1 0) 1 × 2 reconstructed single crystal surfaces, Surf. Sci. 526 (3) (2003) 323–331.

[69] M.M. Biener, C.M. Friend, Heteroepitaxial growth of novel MoO3 nanostructures on Au(1 1 1), Surf. Sci. 559 (2–3) (2004) 173–179.

[70] R.P. Galhenage, H. Yan, S.A. Tenney, N. Park, G. Henkelman, P. Albrecht, D. R. Mullins, D.A. Chen, Understanding the nucleation and growth of metals on TiO_2: Co compared to Au, Ni, and Pt, J. Phys. Chem. C 117 (14) (2013) 7191–7201.

[71] R.P. Galhenage, H. Yan, A.S. Ahsen, O. Ozturk, D.A. Chen, Understanding the growth and chemical activity of Co-Pt bimetallic clusters on TiO_2(110): CO adsorption and methanol reaction, J. Phys. Chem. C 118 (31) (2014) 17773–17786.

[72] Z.J. Wang, F. Yang, S. Axnanda, C.J. Liu, D.W. Goodman, Preparation and characterization of Co-Rh bimetallic model catalysts: from thin films to dispersed clusters, Appl. Catal. A Gen. 391 (1–2) (2011) 342–349.

[73] M. Li, E.I. Altman, Cluster-size dependent phase transition of Co oxides on Au (111), Surf. Sci. 619 (2014) 6–10.

[74] U. Diebold, J.M. Pan, T.E. Madey, Ultrathin metal films on TiO_2(110): metal overlayer spreading and surface reactivity, Surf. Sci. 287-288 (PART 2) (1993) 896–900.

[75] M.D. Porosoff, W. Yu, J.G. Chen, Challenges and opportunities in correlating bimetallic model surfaces and supported catalysts, J. Catal. 308 (2013) 2–10.

[76] S. Han, K. Shin, G. Henkelman, Buddie Mullins, C. selective oxidation of acetaldehyde to acetic acid on Pd-Au bimetallic model catalysts, ACS Catal. 9 (5) (2019) 4360–4368.

[77] S. Kattel, W. Yu, X. Yang, B. Yan, Y. Huang, W. Wan, P. Liu, J.G. Chen, CO 2 hydrogenation over oxide-supported PtCo catalysts: the role of the oxide support in determining the product selectivity, Angew. Chem, 128 (28) (2016) 8100–8105.

[78] S.A. Tenney, W. He, C.C. Roberts, J.S. Ratliff, S.I. Shah, G.S. Shafai, V. Turkowski, T.S. Rahman, D.A. Chen, CO-induced diffusion of Ni atoms to the surface of Ni-Au clusters on TiO_2(110), J. Phys. Chem. C 115 (22) (2011) 11112–11123.

[79] A. Naitabdi, L.K. Ono, F. Behafarid, B.R. Cuenya, Thermal stability and segregation processes in self-assembled size-selected Au Xfe 1-x nanoparticles deposited on Tio 2(110): composition effects, J. Phys. Chem. C 113 (4) (2009) 1433–1446.

[80] J. Kiss, L. Óvári, L. Bugyi, A. Berkó, Characterization of Au-Rh and Au-Mo bimetallic nanoclusters on TiO 2(110): a comparative study, React. Kinet. Catal. Lett. 96 (2) (2009) 391–396.
[81] R.P. Galhenage, K. Xie, H. Yan, G.S. Seuser, D.A. Chen, Understanding the growth, chemical activity, and cluster-support interactions for Pt-Re bimetallic clusters on TiO_2(110), J. Phys. Chem. C 120 (20) (2016) 10866–10878.
[82] S. Blomberg, N. Johansson, E. Kokkonen, J. Rissler, L. Kollberg, C. Preger, S. M. Franzén, M.E. Messing, C. Hulteberg, Bimetallic nanoparticles as a model system for an industrial NiMo catalyst, Materials (22) (2019) 12.
[83] C. Ranga, V.I. Alexiadis, J. Lauwaert, R. Lødeng, J.W. Thybaut, Effect of Co incorporation and support selection on deoxygenation selectivity and stability of (Co)Mo catalysts in anisole HDO, Appl. Catal. A Gen. 571 (2019) 61–70.
[84] R. Singh, D. Kunzru, S. Sivakumar, Co-Promoted MoO3 nanoclusters for hydrodesulfurization, Catal. Sci. Technol. 6 (15) (2016) 5949–5960.
[85] A. Sridhar, M. Rahman, A. Infantes-Molina, B.J. Wylie, C.G. Borcik, S.J. Khatib, Bimetallic Mo-Co/ZSM-5 and Mo-Ni/ZSM-5 Catalysts for methane dehydroaromatization: a study of the effect of pretreatment and metal loadings on the catalytic behavior, Appl. Catal. A Gen. 589 (2020), 117247.
[86] V.R. Surisetty, A.K. Dalai, J. Kozinski, synthesis of higher alcohols from synthesis gas over Co-promoted alkali-modified MoS_2 catalysts supported on MWCNTs, Appl. Catal. A Gen. 385 (1–2) (2010) 153–162.
[87] S. Kim, M.C. Kim, S.H. Choi, K.J. Kim, H.N. Hwang, C.C. Hwang, Size dependence of Si 2p core-level shift at Si nanocrystal/Si O2 interfaces, Appl. Phys. Lett. (2007).
[88] S. Peters, S. Peredkov, M. Neeb, W. Eberhardt, M. Al-Hada, Size-dependent XPS spectra of small supported Au-clusters, Surf. Sci. (2013).
[89] J. Kibsgaard, K. Morgenstern, E. Lægsgaard, J.V. Lauritsen, F. Besenbacher, Restructuring of cobalt nanoparticles induced by formation and diffusion of monodisperse metal-sulfur complexes, Phys. Rev. Lett. 100 (11) (2008), 116104.
[90] J.V. Lauritsen, M.V. Bollinger, E. Lægsgaard, K.W. Jacobsen, J.K. Nørskov, B. S. Clausen, H. Topsøe, F. Besenbacher, Atomic-scale insight into structure and morphology changes of MoS 2 nanoclusters in hydrotreating catalysts, J. Catal. 221 (2) (2004) 510–522.
[91] S. Krishnamurthi, M. Farmanbar, G. Brocks, One-dimensional electronic instabilities at the edges of MoS_2, Phys. Rev. B (16) (2020) 102.
[92] S. Krishnamurthi, G. Brocks, 1D metallic states at 2D transition metal dichalcogenide semiconductor heterojunctions, npj 2D Mater. Appl. (1) (2021) 5.
[93] M. Bravo-Sanchez, A. Romero-Galarza, J. Ramírez, A. Gutiérrez-Alejandre, D. A. Solís-CASados, Quantification of the sulfidation extent of Mo in Co-Mo HDS catalyst through XPS, Appl. Surf. Sci. 493 (2019) 587–592.